Ceramics-Silikáty 62 (4), 355-363 (2018)
www.ceramics-silikaty.cz doi: 10.13168/cs.2018.0031

REFRACTORY CERAMICS SYNTHESIS BY SOLID-STATE REACTION BETWEEN $CaCO_3$ (MOLLUSK SHELL) AND Al_2O_3 POWDERS

#JOSÉ G. MIRANDA-HERNÁNDEZ*, MAYAHUEL ORTEGA-AVILÉS**, HÉCTOR HERRERA-HERNÁNDEZ*, CARLOS O. GONZÁLEZ-MORÁN*, GEORGINA GARCÍA-PACHECO***, ENRIQUE ROCHA-RANGEL****

*Universidad Autónoma del Estado de México, Centro Universitario UAEM Valle de México, Laboratorio de Investigación y Desarrollo de Materiales Industriales, Atizapán de Zaragoza, Estado de México, México
**Instituto Politécnico Nacional, CNMN, Ciudad de México, México
***Instituto Politécnico Nacional, ESIME TICOMAN, Ciudad de México, México
****Universidad Politécnica de Victoria, Departamento de postgrado, Ciudad Victoria, Tamaulipas, México

#E-mail: jgmirandah@uaemex.mx

Submitted June 19, 2018; accepted September 11, 2018

Keywords: Refractories, Calcite, Alumina, Snail shells (mollusk shells), Refractory calcium aluminate ceramics, Sintering process, Mechanical properties, Thermal shock resistance

Calcium aluminate-based refractory ceramic was developed as an innovative refractory material, using garden snail (Helix aspersa) shells as a natural source of $CaCO_3$. A 1:1 molar ratio mixture of $CaCO_3$ from snail shells and commercial Al_2O_3 powder was prepared by means of high-energy mechanical milling. The mixed powder was compacted in cylindrical samples (disks) and consolidated by sintering at 1450°C and 1500°C for 1h. The density and porosity were evaluated using the Archimedes principle, while the mechanical properties (hardness, fracture toughness, and shear modulus) were determined by indentation and ultrasonic methods, respectively. The thermal shock resistance was tested by heating samples to temperatures between 900 and 1400°C and subsequent quenching in water at room temperature. X-ray diffraction patterns of sintered samples indicate the formation of different calcium aluminate phases, such as $CaAl_{12}O_{19}$ (krotite/monoclinic), $CaAl_4O_7$ (grossite/monoclinic) and $CaAl_2O_4$ (hibonite-5H/hexagonal). The fracture toughness and shear modulus values of materials sintered at 1450°C were higher (0.48 MPa·$m^{1/2}$ and 59 GPa, respectively) than those of materials sintered at 1500°C (0.43 MPa·$m^{1/2}$ and 55 GPa, respectively). Also changes in the bulk density, hardness and thermal shock resistance values were observed in materials sintered at 1450°C and 1500°C.

INTRODUCTION

Biomineralization refers to a natural process for the formation of organic-inorganic minerals by means of a living organism, such as calcium carbonate, calcium phosphate, silica, iron oxide, hydroxyapatite, and others [1-3]. The main interest of these minerals is the innovation in their applications to improve durability and reinforcement of concrete-buildings, remediation of environment as water or soil, and also as bone-replacement in dentistry and orthopedics (i.e. implants devices) [1, 2], other minerals as ZnO crystals have been used as semiconductors and photocatalysts [4]. $CaCO_3$ biomineralization produces three different biological phases of calcium carbonate as anhydrous polymorphs, viz. calcite, aragonite and vaterite [5-7], $CaCO_3$ is a material that can be used in the restoration of concrete building structures (i.e. reduction of permeability, pore and crack filling, avoiding carbonation) [8]. The calcium can be obtained from corals, fish bones, egg shells or snail shells, etc. which are natural sources due to their advantage of biological origin, as well as reducing of bio-organic waste disposal [9, 10].

The garden snail (*Helix aspersa*), a common gastropod mollusk, is one of the best-known species of snails in the world. In the case of some freshwater snail-shells as *Helisoma trivolis*, *Physa,* and *Biomphalaria glabrata* have about of 95.2 - 98.8 weight % of $CaCO_3$ [11]. The content of calcium carbonate ($CaCO_3$) is around 95 - 99.9 wt. % in freshwater snail shells, the remaining 0.1 - 5 wt. % being organic matter [11-14]. Furthermore, aragonite is the principal inorganic material in snail shells and is decomposed into CaO and CO_2 by upon heating. Thermogravimetric studies of $CaCO_3$ decomposition have been performed to analyze the thermal decomposition kinetics, showing that decomposition occurs between 635°C and 865°C [15], while other studies show that at 871°C $CaCO_3$ needs about 1 hour for complete decomposition [16]. Calcium carbonate polymorphs (aragonite and calcite) obtained from snail shells or egg shells can be useful in biodiesel synthesis [9], in the preparation of hydroxyapatite nanorods for orthopedic

applications [10] and in biocompatibility studies [17]. In other cases, CaO obtained by thermal decomposition of $CaCO_3$ is used to obtain calcium aluminates ($CaO \cdot Al_2O_3$) for concrete and mortars [18] or even as a binder, considering their biocompatibility characteristics with body fluids [19]. Calcium aluminate is the main component of calcium aluminate cement, which is widely used in the construction industry and is a promising candidate as a persistent luminescence material [18]. Calcium aluminate-based cement has also been studied for biomedical applications as endodontics because of their good physical and mechanical properties, as well as its biocompatibility [19, 20].

The aim of the present research is the synthesis of calcium aluminates refractory material by an easy and direct processing route through a chemical solid-state reaction between alumina (Al_2O_3) and calcia (CaO) [18], using $CaCO_3$ from snail (*helix aspersa*) shells as a CaO source to obtain calcium aluminates [16] with favorable physical properties. On the other hand, if the synthesis of these materials turns out to be viable, the authors are will take this research as a reference for a future work on the in-situ synthesis of a calcium aluminate with metallic particles of Al and Ag as reinforcement for the study of the mechanical properties and biocompatibility characteristics for dental applications.

EXPERIMENTAL

$CaCO_3$ obtained from a natural source

A sufficient quantity of snail (*Helix aspersa*) was collected as a raw material of $CaCO_3$ mineral [6, 18] for the synthesis of calcium aluminate. In order to eliminate surface impurities, the snail shells were rinsed with distilled water and isopropyl alcohol and then dried with a flux of hot air. All snail shells were crushed using a porcelain mortar to produce coarse powder, and then this powder was submitted to a heating process at 200°C by 1 hour in an electrical furnace (Yamato FO200CR). Resulting powder was subjected to a dry ball-milling process in a planetary mill (Fritsch Pulverisette 6) during 1 hour at 200 rpm, using an agate container and agate grinding balls (with diameter 10 mm) with a mass ratio of materials and grinding balls of 1:6. The size reduction of the $CaCO_3$ powder was to particle sizes < 100 mesh in average.

Chemical composition and synthesis process

The raw materials used were α-Al_2O_3 powder (< 100 mesh, ≥ 98 % purity, Aldrich) and $CaCO_3$ powder obtained as previously described [3, 11, 14]. The chemical composition formed for the synthesis material is 49.5 wt. % $CaCO_3$ + 50.5 wt. % Al_2O_3 considering a 1:1 molar ratio; the mixture was submitted to a dry ball-milling process for 4 hours at 200 rpm through a high-energy planetary mill (Fritsch Pulverisette 6), using an agate container and agate grinding balls with a ratio between powder- and balls of 1:10. The powder mixture was compacted by uniaxial pressure (300 MPa) at room temperature in the form of cylindrical samples of 20 mm in diameter and 3 mm in thickness (Figure 3). Subsequently the samples were sintered at 1450°C or 1500°C in an air atmosphere, using an electrical furnace (Nabertherm LHT 02/18), with a heating rate of $10°C \cdot min^{-1}$. The heating process was performed in several stages; first, the temperature was elevated and stabilized at 400°C for 20 minutes, then the temperature was elevated to 800°C and stabilized for 20 minutes to remove the organic matter that was not eliminated in the previous stage [21]. After this, the temperature was elevated at 1200°C and stabilized for 20 minutes, assuming the whole decomposition of $CaCO_3$ [15,16]; finally, the temperature was elevated to 1450°C or 1500°C to promote the chemical reaction between CaO and Al_2O_3 in order to obtain the desired refractory material with good density. Figure 1 shows samples before and after sintering; the different color is due to the burnout of organic matter and the chemical reaction that has occurred during sintering.

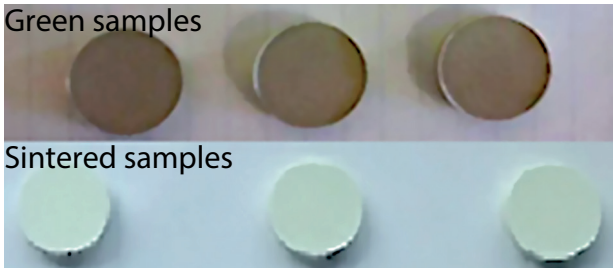

Figure 1. Green samples and samples after sintering process at 1450°C.

Characterization of synthesized materials

The bulk density was determined by the Archimedes' principle. The microstructure was determined by scanning electron microscopy (FEI Quanta 3E FEG) at low vacuum using the backscattered electrons signal. Crystalline phase identification was carried out by means of X-ray diffraction (Panalytical X´Pert-PRO) patterns recorded using Cu radiation (λ_{Cu} = 1.54056 Å) at 40 KV and 40 mA, in the range between $15° \leq 2\theta \leq 100°$ with a step of 0.02°. The mechanical properties such as hardness and fracture toughness were evaluated by using the indentation method (EMCO-TEST DuraScan 20) [22, 23]. Finally, the sintered materials were subjected to a thermal shock resistance test by heating samples to temperatures in the range between 900 and 1400°C (Yamato FO200CR) in intervals of 100°C and subsequent coolling in water at room temperature.

RESULTS AND DISCUSSION

Chemical composition and solid state chemical reactions

Al_2O_3 and snail-shell powder were the raw materials to produce calcium aluminates by solid-state chemical reaction through the sintering process at 1450°C or 1500°C. The X-ray diffraction patterns of Figure 2 confirm that the snail-shell powder is principally $CaCO_3$, identified as calcite and aragonite.

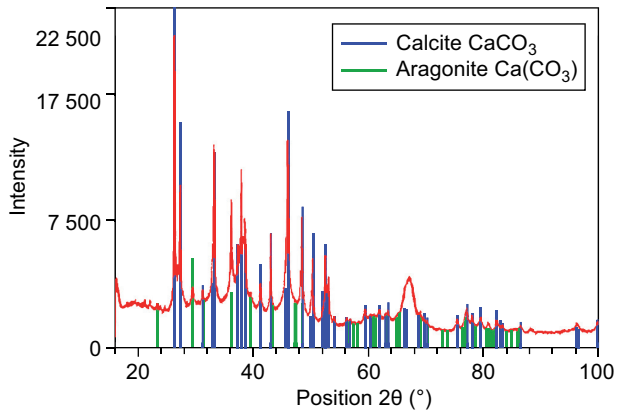

Figure 2. XRD pattern of snail-shell powder.

The compacted samples before and after sintering process were weighted, to determine of the mass loss percentage (α). The values of (α) listed in Table 1 were determined via Equation 1,

$$\alpha = \left(1 - \frac{m_1}{m_0}\right) \times 100\,, \qquad (1)$$

where m_1 is the mass after sintering and m_0 is the mass before sintering.

Of course, the change of mass is due to the decomposition of $CaCO_3$ between approximately 635 and 865°C [15], during which CO_2 gas is formed according to Equation 2, i.e.

$$CaCO_3 \xrightarrow{\Delta} CaO + CO_2\uparrow\,. \qquad (2)$$

Then, a solid state reaction between Al_2O_3 and CaO occurs according to Equation 3, forming calcium aluminate due to the increase in temperature up to 1450°C or 1500°C [18].

$$Al_2O_3 + CaO \xrightarrow{\Delta} CaAl_2O_4\,. \qquad (3)$$

After the sintering process and considering the mass loss (Table 1), the experimental chemical compositions finally formed between Al_2O_3 and CaO are 71.0 wt. % Al_2O_3 + 29.0 wt. % CaO and 70.3 wt. % Al_2O_3 + 29.7 wt. % CaO for samples sintered at 1450 and 1500°C, respectively.

Although the percentages of CaO and Al_2O_3 are slightly different in the two systems, it is approximately 70 % alumina and 30 % calcium oxide; therefore, according to the CaO–Al_2O_3 binary phase diagram, the possible calcium aluminate phases that can form are $CaO{\cdot}Al_2O_3$ ($CaAl_2O_4$/krotite) and $CaO{\cdot}2Al_2O_3$ ($CaAl_4O_7$/grossite), considering the sintering temperatures in each system as shown in Figure 3 [24]. In other work, the formation of the grossite and krotite phases was observed in a heating process at 1300°C [25]. Finally, when $CaCO_3$ is decomposed completely into CaO and CO_2, a sequence of simple reactions [24] or simultaneous multiple reactions occur, leading to the formation of calcium aluminates [26].

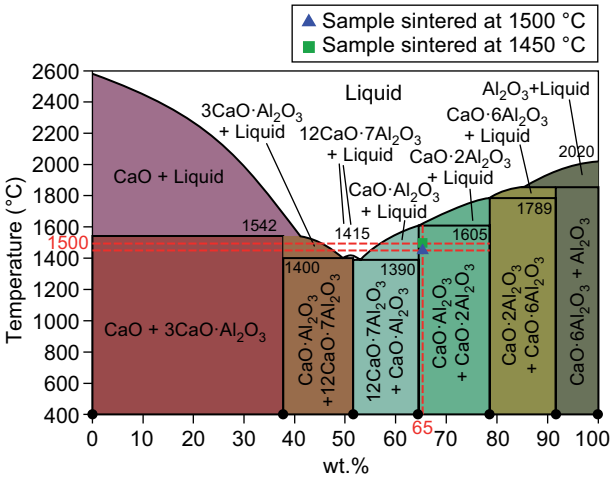

Figure 3. Binary phase diagram of CaO–Al_2O_3 system (wt. % vs. temperature) [24].

Microstructural and structural analysis

Sintered samples were observed by scanning electron microscopy using backscattered electrons to obtain atomic number contrast micrographs, where each gray tone corresponds to a phase with different elemental composition. Figure 4 shows the microstructure obtai-

Table 1. Mass loss of the materials before and after sintering.

Material	Initial mass before sintering (Al_2O_3 + $CaCO_3$)	Final mass after sintering (Calcium aluminate)	Mass loss
Temperature 1450°C	2.473 g	1.758 g	0.71 g → 28.9 %
Temperature 1500°C	2.479 g	1.779 g	0.70 g → 28.2 %

ned after sintering process at 1450°C or 1550°C (with magnifications 800X and 5000X, respectively). In all micrographs 2 or 3 distinguishable gray tones are visible, see Figures 4a through 4d. In particular, Figures 4b and 4d referring to the sample sintered at 1500°C suggest the formation of 3 phases with different chemical composition and a smaller amount of pores than the sample sintered at 1450°C. An interesting detail is that the pores are usually located inside areas with medium gray tone. Finally, is evident that the clear gray areas surround the pores and the darker gray grains grow with characteristic morphologies as can be seen in Figure 4d.

The structural data obtained through XRD analysis of the sintered samples at 1450°C or 1500°C are shown in Figure 5. In these XRD patterns, the absence of CaO and Al_2O_3 confirm the complete reaction between the raw materials. Three crystalline phases have been identified, corresponding to several calcium aluminates, which were formed during sintering: $CaO{\cdot}6Al_2O_3$ ($CaAl_{12}O_{19}$/hibonite) with reference code 00-033-0253, hexagonal crystal system and space group P63/mmc; $CaO{\cdot}2Al_2O_3$ ($CaAl_4O_7$/grossite) with reference code 98-004-4519, monoclinic crystal system and space group C 1 2/c 1, and $CaO{\cdot}Al_2O_3$ ($CaAl_2O_4$/krotite) with reference code 98-018-0997, monoclinic crystal system and space group P 1 21/c 1. According to the chemical composition and the sintering temperatures only the formation of grossite and krotite was expected in both samples on the basis of the CaO-Al_2O_3 equilibrium phase diagram [24, 25]. As far as the presence of hibonite is concerned, the formation of this phase $CaO{\cdot}6Al_2O_3$ ($CaAl_{12}O_{19}$/hibonite) occurs probably during the sintering process because

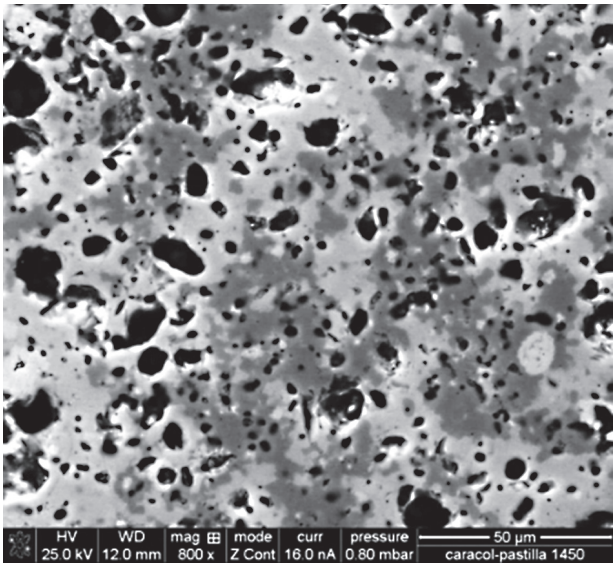

a) 1450°C

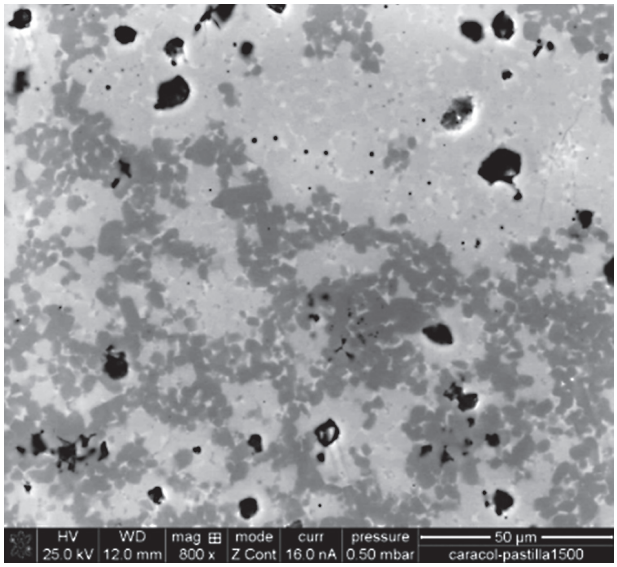

b) 1500°C

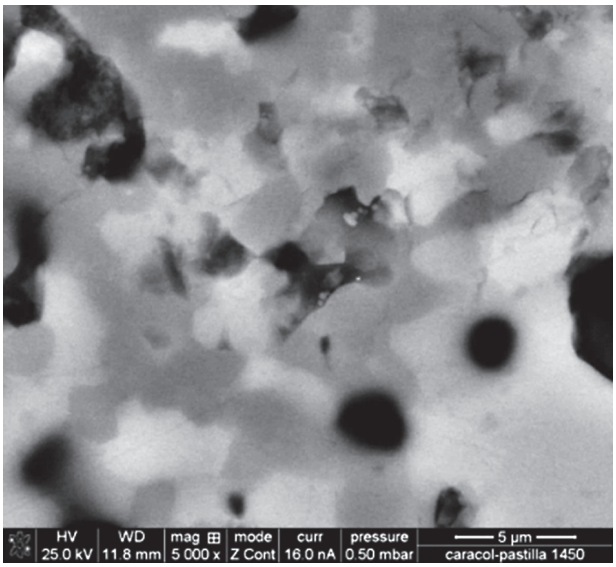

c) 1450°C

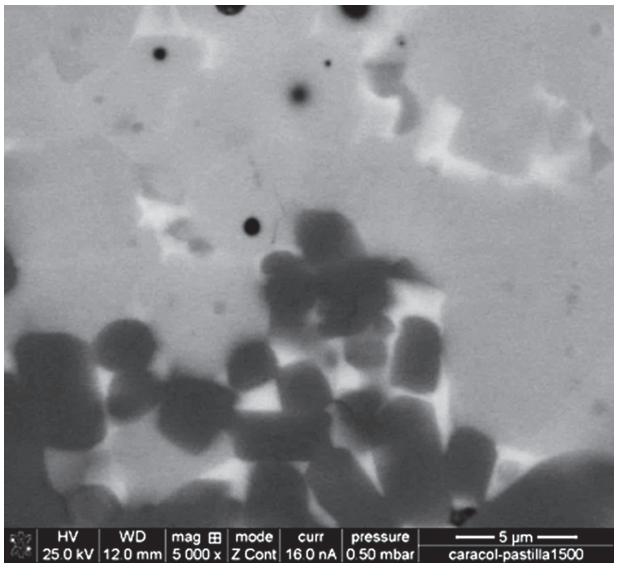

d) 1500°C

Figure 4. Backscattered electron images: a, c) sample sintered at 1450°C and b, d) sample sintered at 1500°C.

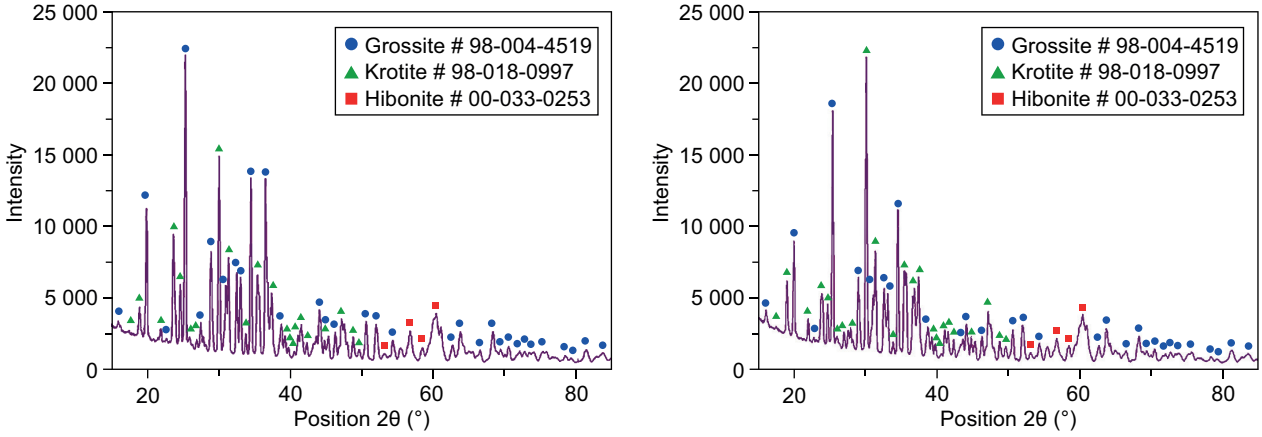

a) Sample 1450°C/1 h

b) Sample 1500°C/1 h

Figure 5. XRD patterns of samples sintered at 1450 °C or 1500 °C.

the compacted samples before heating do not have a uniform distribution of CaO and Al_2O_3 powders; this fact may cause that CaO in local excess concentration reacts with the aluminates already formed. Moreover, taking up again thermodynamic data reported by some authors [24, 27], the first phase formed during sintering process must be hibonite phase ($CaAl_{12}O_{19}$), which is richer in Al_2O_3 content; only after this, grossite ($CaAl_4O_7$), and krotite ($CaAl_2O_4$), which are poorer in Al_2O_3 content, are formed.

Finally, on basis of aluminum and calcium elemental profiles along the white line in Figure 6, it is possible to recognize qualitatively the variation of Al and Ca concentration in areas with different contrast, which are coincident with changes in atomic number contrast on the backscattered electron image. Combining XRD results and elemental profiles obtained by EDS along the white line in Figure 6, one may conclude that the lightest gray areas correspond to hibonite ($CaO{\cdot}6Al_2O_3 = CaAl_{12}O_{19}$), the medium gray areas to grossite ($CaO{\cdot}2Al_2O_3 = CaAl_4O_7$) and the darker gray areas to krotite ($CaO{\cdot}Al_2O_3 = CaAl_2O_4$).

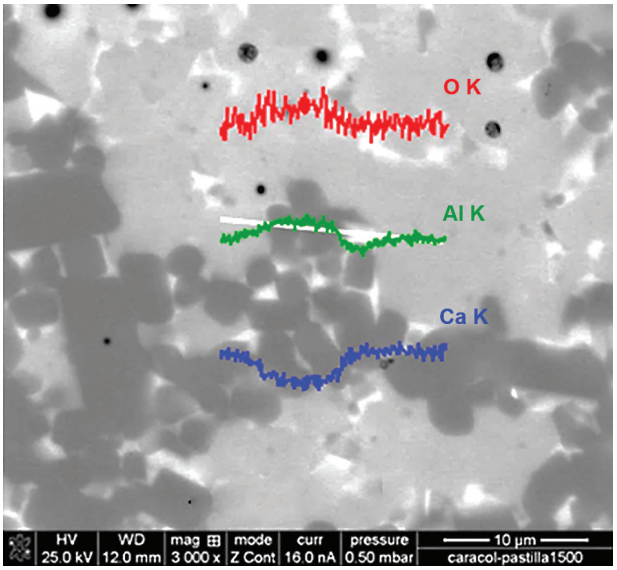

Figure 6. Backscattered electron image of sintered sample at 1500°C, showing elemental profiles along a white line obtained by EDS.

Density and mechanical properties

Bulk density and apparent (open) porosity of the materials synthesized were determined using Archimedes' principle. The results obtained for the sintered materials are shown in Table 2; as expected, the bulk density of 2.88 $g{\cdot}cm^{-3}$, corresponding to the calcium aluminate material sintered at 1500°C, is higher than 2.40 $g{\cdot}cm^{-3}$, determined for the material sintered at 1450°C, because at 1500°C the diffusion coefficients are higher, leading to enhanced densification. Of course, the bulk density is related to the porosity and the shrinkage. As the sintering temperature increases, the bulk density increases, and the porosity decreases (5.4 and 3.0 % respectively); this fact explains why the volumetric shrinkage value shown in Table 2 is higher for the material sintered at 1500°C. In another work [28], a porous ceramic material was processed from commercial Al_2O_3 and commercial $CaCO_3$ by mechanical milling, uniaxial compaction, and sintering. The authors reported an apparent poro-

Table 2. Basic characteristics and mechanical properties of sintered samples.

Property	Sintering temperature	
	1450°C	1500°C
Bulk density ($g{\cdot}cm^{-3}$)	2.40	2.88
Apparent (open) porosity (%)	5.4	3.0
Volumetric shrinkage (%)	42.8	49.5
Hardness (GPa)	5.8 ± 0.3	8.4 ± 0.2
Fracture toughness K_{IC} ($MPa{\cdot}m^{1/2}$)	0.49 ± 0.04	0.43 ± 0.07
Shear modulus (GPa)	59 ± 1	55 ± 2

sity of more than 20 %, with an average pore size of 1 μm, while the apparent porosity in the materials of the present work, sintered at 1450°C and 1500°C is 5.4 and 3.0 % respectively, with pore sizes between 0.5 and 20 micrometers.

Indentation tests were applied to evaluate the hardness and fracture toughness of the synthesized materials. It was found the material sintered at 1450°C and 1500°C have hardness values of 5.8 ± 0.3 GPa and 8.4 ± 0.2 GPa, respectively.

The fracture toughness (K_{IC}) was calculated from using the mathematical models of Lawn-Evans-Marshall [29], Lawn-Fuller [30], Evans-Charles [31], Anstis-Chantikul-Lawn-Marshall [32], Japanese International Standard (JIS) [33], and Niihara-Morena-Hasselman [34]. All the values determined for these materials are low, with a consistent tendency for the different mathematical models as is shown in Figure 7. The Lawn-Evans-Marshall model gives the lowest fracture toughness and the Niihara-Morena-Hasselman model the largest fracture toughness values for both samples. As is known, if the fracture toughness value is low for any material, this material is sensitive to mechanical flaws when is submitted to mechanical stresses such as tension, vibration, and impact. The values of K_{IC} presented in Table 2 for both materials, namely 0.49 MPa·m$^{1/2}$ for the material sintered at 1450°C and 0.43 MPa·m$^{1/2}$ for the material sintered at 1500°C, are average values of the fracture toughness determined by all these mathematical models [35-38]. The low K_{IC} values indicate that the synthesized materials are very brittle and sensitive to mechanical flaws. Similarly, low fracture toughness values, determined by the Vickers indentation technique, have been reported in hydroxyapatite ceramics and PLZT sensor materials [39, 40]. The sample sintered at 1500°C has slightly lower fracture toughness values than the sample sintered at 1450°C, which indicates that the denser material is even more brittle than the porous one.

The shear modulus was measured by ultrasonic technique according to relation $\mu = \rho\varepsilon^2$, where μ is the shear modulus, ρ is the bulk density of the materials, and ε is the transversal sound velocity measured in the materials [32]. These values are 59 ± 1 GPa and 55 ± 2 GPa for samples sintered at 1450°C and 1500°C, respectively, see Table 2. For comparison, other researchers reported a shear modulus of 126 GPa in $CaAl_4O_7$ refractory cement (Al_2O_3/CaO molar relation 1.41) [41].

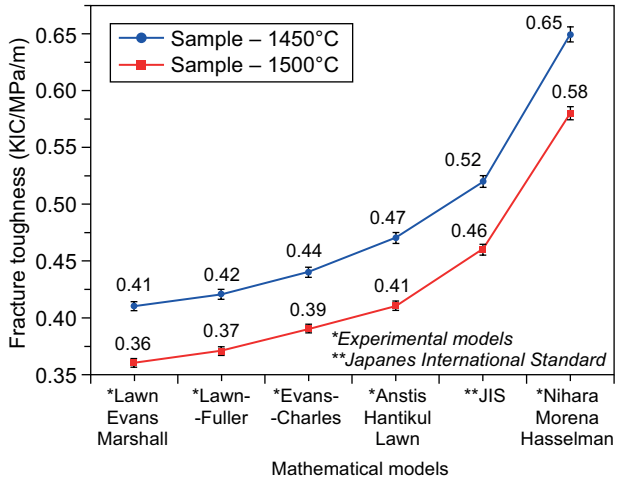

Figure 7. Fracture toughness values calculated by means of several mathematical models.

Thermal shock resistance

Thermal shock resistance on the samples was evaluated, and the change in the flaw generation in the calcium aluminates refractory materials during these tests was observed via optical microscopy. Figures 8a, 8c, and 8e correspond to samples sintered at 1450°C, while Figures 8b, 8d, and 8f correspond to samples sintered at 1500°C, respectively. These images show sample surfaces after being submitted to different temperatures during hea-

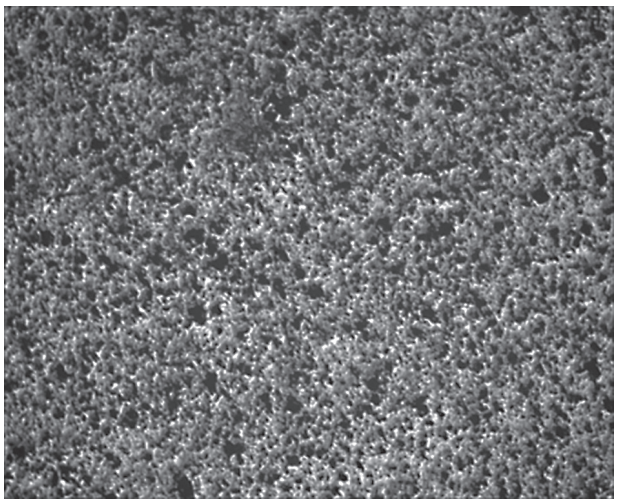

a) 1450°C

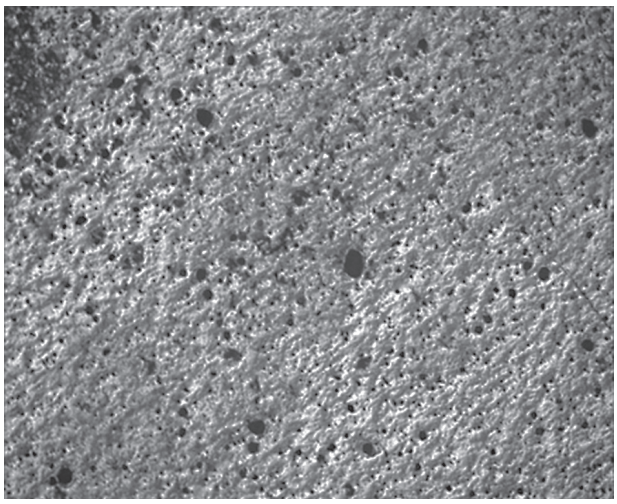

b) 1500°C

Figure 8. Surface of samples sintered at 1450°C and 1500°C after thermal shock tests from 900°C (a) and (b). *Continue on next page.*

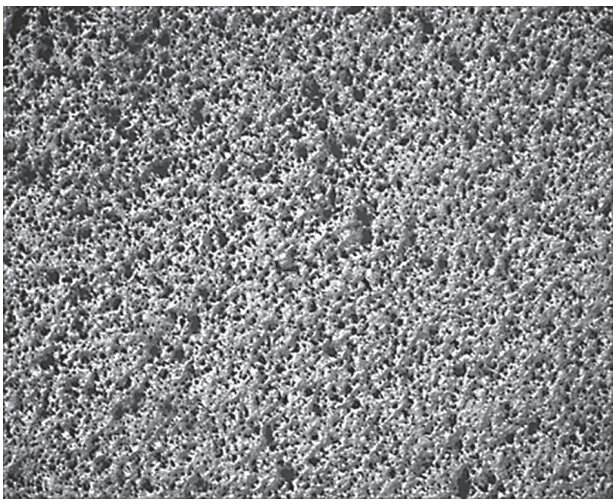

c) 1450°C

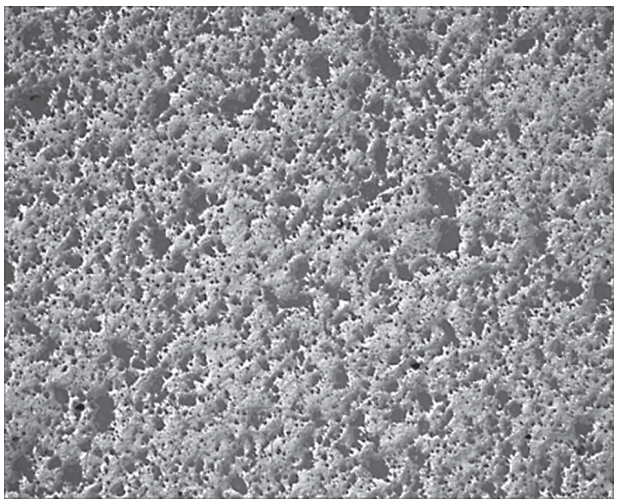

e) 1450°C

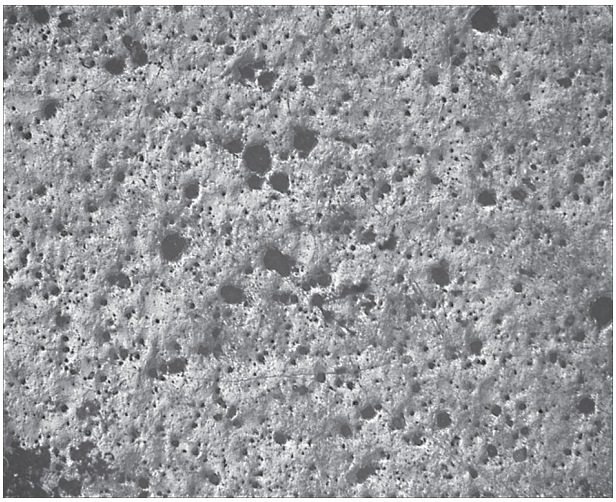

d) 1500°C

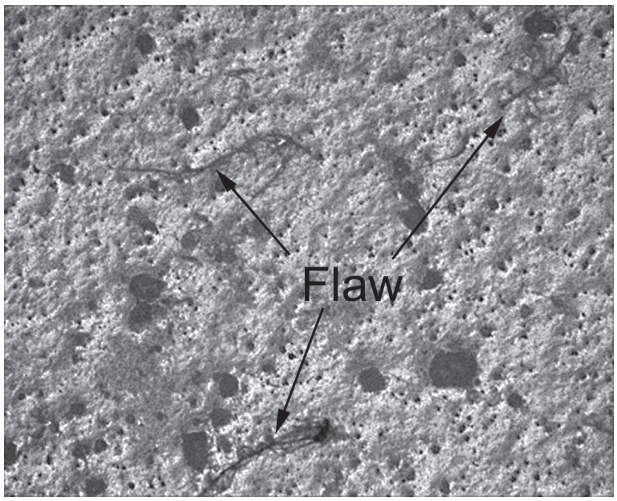

f) 1500°C

Figure 8. Surface of samples sintered at 1450°C and 1500°C after thermal shock tests from 1000°C (c) and (d) and 1100°C (e) and (f).

ting (900, 1000 and 1100°C, respectively) and rapidly cooled (quenched) in water to room temperature (21°C). Figures 8a, 8b, 8c and, 8d do not reveal significant changes when the materials are submitted a thermal shock at 900 and 1000°C. However, a significant change is observed in the microstructure of the material sintered at 1500°C, when the refractory material is heated to 1100°C and subsequently quenched, as is evident from the mechanical flaws shown in Figure 8f.

The flaws observed in Figure 8f considered as thermal shock flaws just occur in the refractory material sintered at 1500°C, this fact is not observed in the microstructure of the material sintered at 1450°C as shown in Figure 9. Therefore, the material synthesized at 1450°C is the better refractory due to that the porosity has an effect on thermal shock cracking, considering the crack deflection and the crack arresting caused by pores because of energy dissipation during fracture caused by thermal effects [42].

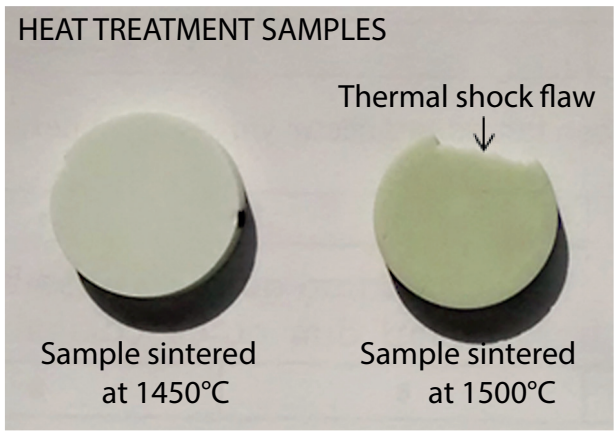

Figure 9. Samples sintered at 1450°C and 1500°C, after thermal shock tests.

CONCLUSIONS

The synthesis of calcium aluminate refractory materials by *in-situ* solid state reaction between Al_2O_3 and $CaCO_3$ obtained from snail shells is feasible. During the sintering process, the $CaCO_3$ is decomposed into CaO and CO_2. As soon as CaO is available to react with Al_2O_3 calcium aluminate formation occurs and results in three different phases that were identified by XRD as $CaO{\cdot}6Al_2O_3$ ($CaAl_{12}O_{19}$/hibonite), $CaO{\cdot}2Al_2O_3$ ($CaAl_4O_7$/grossite), and $CaO{\cdot}Al_2O_3$ ($CaAl_2O_4$/krotite). The formation of hibonite probably occurs during the sintering process, because the compacted samples before heating do not have a uniform distribution of CaO and Al_2O_3 powders.

The sintering temperature has an important effect on the microstructure and properties of calcium aluminate refractory materials during the sintering process, mainly the bulk density, porosity, and shrinkage. Materials sintered at 1500°C exhibit higher bulk density (i.e. lower porosity) and higher shrinkage. Hardness and shear modulus are appropriate, but the fracture toughness is very low, i.e. the materials are very brittle. Thermal shock tests and subsequent flaw analyses indicate that the calcium aluminate refractory material sintered at 1450°C performs slightly better than the material obtained by sintering at 1500°C, although the reasons are not clear.

Acknowledgments

The research work team "Manufactura y Desarrollo de Materiales Multifuncionales" of the Universidad Autónoma del Estado de México, Instituto Politécnico Nacional and Universidad Politécnica de Victoria appreciates the collaboration and infrastructure support of these Institutions. The authors also wish to thank PFCE-SEP 2018 program by the given support.

REFERENCES

1. Chen Z.W., Li Z.H., Lin Y.H., Yin M.L., Ren J.S., Qu X.G. (2013): Biomineralization inspired surface engi-. neering of nanocarriers for pH-responsive, targeted drug delivery. *Biomaterials*, *34*, 1364-1371. doi:10.1016/j.biomaterials.2012.10.060
2. Takashi K., Ayae S., and Hosoda N. (2002): Calcium Carbonate-Organic Hybrid Materials. *Advanced Materials*, *14*(12), 869-877. doi:10.1002/1521-4095(20020618)14:12<869::AID-ADMA869>3.0.CO;2-E
3. Marin F. and Luquet G. (2004): Molluscan shell proteins, *Comptes Rendus Palevol*, *3*, 462-492. doi:10.1016/j.crpv.2004.07.009
4. Shunichi M., Yoshimasa H., Tatsuya N., Hideki S., Takashi K. (2016): Biomineralization-inspired preparation of zinc hydroxide carbonate/polymer hybrids and their conversion into zinc oxide thin film photocatalysts. *Chemistry-A European Journal*, *22*, 7094-7101. doi:10.1002/chem.201600141
5. Zan G.T., and Wu Q.H. (2016): Biomimetic and bioinspired synthesis of nanomaterials/nanostructures. *Advanced Materials*, *28*, 2099-2147. doi:10.1002/adma.201503215
6. Nico A. J. M. S. and Gijsbertus D.W. (2008): Biomimetic $CaCO_3$ Mineralization using Designer Molecules and Interfaces. *Chemical Reviews*, *108*(11), 4499-4550. doi:10.1021/cr078259o
7. Navdeep K.D., Mondem S.R., Abhijit M. (2013): Biomineralization of calcium carbonate polymorphs by the bacterial strains isolated from calcareous sites. *Journal of Microbioly and Biotechnology*, *23*, 707-714. doi:10.4014/jmb.1212.11087
8. Alonso M.J.C., Ortiz C.E.L., Perez S.O.G., Narayanasamy R., San Miguel G.J.F., Herrera H.H., Balagurusamy N. (2018): Improved strength and durability of concrete through metabolic activity of ureolytic bacteria. *Environmental Science and Pullution Research*, *25*, 21451-21458. doi:10.1007/s11356-017-9347-0
9. Viriya E.N., Krasae P., Puttasawat B., Yoosuk B., Chollacoop N., Faungnawakij K. (2010): Waste shell of mollusk and egg as biodisel production catalysts. *Bioresourse Technology*, *101*, 3765-3767. doi: 10.1016/j.biortech.2009.12.079
10. Suresh K.G., Sathish L., Govindan R., Girija E.K. (2015): Utilization of sanil shells to synthesise hydroxyapatite nanorods for orthopedic applications. *Royal Society of Chemistry Advances*, *5*, 39544-39548. doi:10.1039/C5RA04402B
11. White M.M., Chejlava M., Fried B., Sherma J. (2007): The concetration of calcium carbonate in shells of freshwater snails", *American Malacological Bulletin*, 22, 1, 139-142. doi:10.4003/0740-2783-22.1.139
12. Marxen J.C., Becker W., Finke D., Hasse B., Epple M. (2003): Early mineralization in Biomphalaria glabrata: Microscopic and structural result. *Journal Molluscan Studies*, *69*, 113-121. doi: 10.1093/mollus/69.2.113
13. Ligaszewski M., Surówka K., Stekla J. (2009): The Shell Features of Cornu aspersum (Synonym *Helix aspersa*) and *Helix pomatia*: Characteristics and Comparison. *American Malacological Bulletin*, *27*, 173-181. doi:10.4003/006.027.0215
14. Pokroy B., Fitch A.N., Zolotoyabko E. (2007): Structure of Biogenic Aragonite ($CaCO_3$). *Crystal Growth & Desing*, *7*(9), 1580-1583. doi:10.1021/cg060842v
15. Halikia I., Zoumpoulakis L., Christodoulou E., Pratis D. (2001): Kinetic study of the thermal decomposition of calcium carbonate by isothermal methods of analysis. *The European Journal of Mineral Processing and Environmental Protection*, *1*, 89-102.
16. Galan I., Glasser F. P., Andrade C. (2013): Calcium Carbonate decomposition. *Journal Thermal Analysis and Calorimetry*, *111*, 1197-1202. doi: 10.1007/s10973-012-2290-x
17. Singh A., Purohit K.M. (2011): Chemical Synthesis, Characterization and Bioactivity Evaluation of Hydroxyapatite Prepared from Garden snail (Helix aspersa). *Journal of Bioprocessing & Biotechniques*, *1*, 1-5. doi:10.4172/2155-9821.1000104
18. Tian Y.P., Pan X.L., Yu H.Y., Tu G.F. (2016): Formation mechanism of calcium aluminate compounds base on high-temperature solid-state reaction. *Journal of Alloys and Compounds*, *670*, 96-104. doi: 10.1016/j.jallcom.

2016.02.059
19. Regina de Oliveira I., Luana de Andrade T., Martins R.P., Jacobovitz M., Pandolfelli V.C. (2015): Characterization of Calcium Aluminate Cement Phases when in Contact with Simulated Body Fluid. *Materials Research*, *18*(2), 382-389. doi:10.1590/1516-1439.336714
20. Gamero A.F., Garcia L.F.R., Pires de Souza F.C.P. (2012): Biocompatibility of new calcium aluminate cement (EndoBinder). *Journal of Endodontics, 38*(3), 367-371. doi:10.1016/j.joen.2011.11.002
21. Živcová Z., Gregorová E., Pabst W. (2010): Low-and High-temperature Processes and Mechanisms in the Preparation of Porous Ceramics via Starch Consolidation Casting. *Starch, 62,* 3-10. doi: 10.1002/star.200900139
22. Pramanick A.K. (2015): Evaluation of fracture toughness of sintered silica-nickel nanocomposites. *International Journal of Research in Engineering and Technology*, *4*, 234-239. doi: 10.15623/ijret.2015.0403057
23. Rickhey F., Pandian M.K., Haeng LJ., Lee H., Hee H.J. (2015): Evaluation of the fracture toughness of brittle hardening materials by Vickers indentation. *Engineering Fracture Mechanics*, *148*, 134–144. doi:10.1016/j.engfracmech.2015.09.028
24. Miskufova A., Havlik T., Bitschnau B., Kielski A., Pomadowski H. (2015): Properties of CaO Sintered With Addition of Active Alumina. *Ceramics–Silikáty*, *59(*2), 115-124.
25. Rivas M.J.M., De Aza A.H., Pena P. (2005): Synthesis of $CaAl_2O_4$ from powders: Particle size effect. *Journal of the European Ceramic Society*, *25*, 3269–3279. doi:10.1016/j.jeurceramsoc.2004.06.021
26. Kuzmenko V.V., Uspenskaya I.A., Rudnyi E. B. (1997): Simultaneous Asssessment of Thermodynamic Functions of calcium Aluminates. *Bulletin des Sociét*és *Chimiques Belges*, *106*, 235-243.
27. Eliezer I., Eliezer N., Howalt R.A., Viswanadham P. (1981): Thermodinamic properties of Calcium Aluminates. *The Journal of Physical Chemistry*, *85*(1)9, 2835-2838. doi:10.1021/j150619a028
28. Regina de Oliveira I., Marques C. L.V, Vargas P.L. M.P., Salomão R. (2015): Production of porous ceramic material using different sources of alumina and calcia. Revista Materia, 20(3), 739-746. doi: 10.1590/S1517-707620150003.0078
29. Lawn B. R., Evans A. G. and Marshall D. B. (1980): Elastic/plastic indentation damage in ceramics: the median/radial crack system. *Journal of the American Ceramic Society*, *63*, 574–581. doi:10.1111/j.1151-2916.1980.tb10768.x
30. Lawn H. R. and Fuller E. R. (1975): Equilibrium penny-like cracks in indentation fracture. Journal of Materials Science, 10, 2016–2024.
31. Evans, A. G., Charles E. A. (1976): Fracture toughness determinations by indentation. *Journal of the American Ceramic Society,59*, 371–372. doi:10.1111/j.1151-2916.1976.tb10991.x
32. Anstis G. R., Chantikul P., Lawn, B. R., Marshall, D. B. (1981): A critical evaluation of indentation techniques for measuring fracture toughness: I, Direct crack measurements. *Journal of the American Ceramic Society, 64*, 533–538. doi:10.1111/j.1151-2916.1981.tb10320.x
33. JIS R-1607. (1990): Testing method for fracture toughness of high performance ceramics. Japanease Standards Association.
34. Niihara K., Morena R., Hasselman D. P. H. (1982): Evaluation of KIc of brittle solids by the indentation method with low crack-to-indent ratios. *Journal of Materials Science Letter, 1,* 13–16. doi: 10.1007/BF00724706
35. Fjodor S., Maksim A. (2006): Comparative study on indentation fracture toughness measurements of cemented carbides. *Estonian Journal of Engineering*, *12*, 388-398
36. Moradkhani A., Baharvandi H., Tajdari M., Latifi H., Martikainen J. (2013): Determination of fractue toughness using the area of micro-crack tracks left in brittle materials by Vickers indentation test. *Journal of Advanced Ceramics, 2(*1), 87-102. doi:10.1007/s40145-013-0047-z
37. Pramanick A.K. (2015): Evaluation of fracture toughness of sintered silicanickel nanocomposites. *International Journal of Research in Engineering and Technology*, *4*(3), 334-339. doi: 10.15623/ijret.2015.0403057
38. Miranda H.J.G., Vázquez B.M., Herrera H.H., González M.C.O., Rocha R.E., Refugio G.E. (2016): Tenacidad a la fractura de compuestos cermets $3Al_2O_3$*$2SiO_2$/Ag manufacturados por molienda de alta energía. *Revista Materia*, *21*(1), 243-251. doi:10.1590/S1517-707620160001.0022
39. González M.C.O., Miranda H.J.G., Flores C.J.J., Suaste G.E., Herrera H.H. (2017): A PLZT Novel Sensor with Pt Implanted for Biomedical Application: Cardiac Micropulses Detection on Human Skin. *Advances in Materials Science and Engineering*, *2054940*, 1-7. doi:10.1155/2017/2054940
40. Mishra A., Khobragade N., Sikdar K., Chakraborty S., Bhusan K.S., and Roy D. (2017): Study of Mechanical and Tribological Properties of Nanomica Dispersed Hydroxyapatite Based Composites for Biomedical Applications. *Advances in Materials Science and Engineering*, *9814624*, 1-9. doi: 10.1155/2017/9814624
41. Tchamba A.B., Sofack J.C., Yongue R., Meloa U.C. (2015): Formulation of calcium dialuminate ($CaO·2Al_2O_3$) refractory cement from local bauxite. *Journal of Asian Ceramic Societies*, *3*, 164-172. doi: 10.1016/j.jascer.2015.01.001
42. Xinxin J., Limin D., Qin L., Hui T. Ning L., Qiang Q. (2016): Thermal Shock Cracking of Porous ZrB-SiC Ceramics. *Ceramic International*, *22*, 11, 13309-13313. doi:10.1016/j.ceramint.2016.05.040